Tomographic imaging of a carbonate core using different ultrasonic seismic sources at the laboratory scale : piezoelectric vs point-like pulsed-laser

Chengyi Shen, Daniel Brito, Julien Diaz, Clarisse Bordes, Jean Virieux, Stéphane Garambois

Tomographic imaging of a carbonate core using different ultrasonic seismic sources at the laboratory scale : piezoelectric *vs* point-like pulsed-laser

Chengyi Shen, Daniel Brito, Julien Diaz and Clarisse Bordes, Université de Pau et des Pays de l'Adour, E2S UPPA, CNRS, Total, LFCR; Jean Virieux and Stéphane Garambois, ISTerre, Université Grenoble Alpes*

SUMMARY

Carbonate rocks are of particular interest in exploration geophysics due to the prosperity of carbonate reservoirs in oil & gas industry. Such rocks are generally heterogeneous, anisotropic, porous and fractured, with complicated sedimentary compositions. Imaging their petrophysical properties can therefore be challenging with classical techniques. We propose here to proceed to the V_p seismic tomographic imaging of a circular section of a carbonate core of diameter 10.7 cm based on the first arrival travel times of seismic waves. A point-like pulsed-laser and a piezoelectric transducer are alternatively used as seismic sources and a laser vibrometer records the travelling waves at the periphery of the carbonate core. V_p images obtained with both sources are then analyzed and compared to an X-ray CT-scan tomography.

INTRODUCTION

Reproduction of seismic explorations at laboratory scale (Bretaudeau et al., 2011; De Cacqueray et al., 2011; Holzhauer et al., 2017) is a promising approach that could lead to significant progress in the development and evaluation of imaging methods for complex media, such as monitoring at the near-surface and the crust scales, especially in case that difficulties are encountered during quantitative analyses on seismic exploration data. Besides, a high-resolution seismic dataset recorded in laboratory can reveal small-scale geophysical properties such as elastic wave velocities, porosity or permeability that could be efficiently retrieved by numerical inversions on seismic attributes (Dupuy et al., 2016a,b). To some extent, results obtained at laboratory scale may be transferred to the field scale through upscaling methods (Backus, 1962; Tiwary et al., 2009; Capdeville et al., 2010; Dvorkin and Wollner, 2017; Bailly et al., 2019). The quality of the inversion relies strongly on seismic attributes estimations, which in turn depends on several factors such as the seismic source quantification, the sensitivity of the receivers and the acquisition setup (Dupuy et al., 2016a). Seismic tomography is one of the widely-used inversion methods to image the interior of geological elements at various scales. In this work we proceed to a high-resolution V_p seismic tomography of a carbonate core using an original experimental set-up where two kind of seismic sources are successfully used (pulsed-laser and piezoelectric transducer) and a moving laser vibrometer acts as receivers.

X-RAY CT-SCAN

The carbonate core of 10.7 cm in diameter used in the present study was first processed in TOTAL CSTJF (Centre Scientifique et Technique Jean Féger) by means of X-ray CT-scan tomography through a medicine scanner from *General Electric*'s Discovery® series. Fig. 1 displays the image of one slice from the CT-scan dataset, the spatial resolution being $\sim$260 μm. The color scheme reveals the linear attenuation coefficients scaled to the color range [0, 255]. Red colors imply stronger X-ray attenuation while blue color weaker ones. The slice shows a relatively high contrast between the light-red side and the blue side, the latter indicating lower density or/and stronger porosity given the associated weaker attenuation. We focus on probing this core slice with ultrasounds.

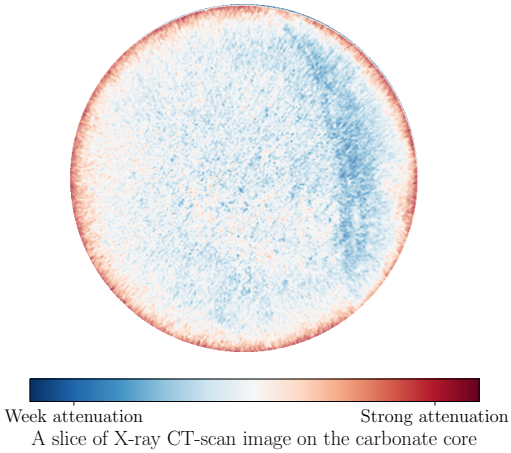

Figure 1: CT-scan tomography slice of the carbonate core. The slice features a moon-like area on the right and appears to be heterogeneous. The CT-scan images manifests the "beam hardening" artifact (Ketcham and Carlson, 2001) forming the "red ring" around the core, which is the most common default of an uncorrected X-ray CT-scan reconstruction.

EXPERIMENTAL SET-UP

We developed an experimental prototype allowing dense seismic scanning around core samples under a cylindrical coordinate system. After experimental calibrations on an aluminum core (Shen, 2020), the angular error of the prototype's rotational platform was estimated to be less than 1° per cycle.

Two types of seismic source are used in the laboratory-scale experimentation: a piezoelectric source (PZT hereafter, effective diameter = 10 mm, central frequency $f_c \approx 0.5$ MHz) and a pulsed-laser source (PL hereafter, diameter $\ll 1$ mm, $f_c \approx 1$ MHz). Despite the availability and simplicity of PZT sources for laboratory-scale geophysical experiments, those planar sources are not ideal to stick them correctly on the curved surface of a cylinder core, even harder to guarantee the stability of the

PZT on the surface to ensure a constant and reproducible coupling. Another important constraint of the PZT sources lays in the seismic field measurement uncertainty induced by the relative large size effect of the source as compared to the wavelength (Dellinger and Vernik, 1994). In terms of numerical modelling, a PZT may not be always simplified to a point-source, adding some difficulties to the source representation when accurate wave propagation modeling is expected.

In order to overcome the disadvantages of the conventional PZT sources, Scales and Malcolm (2003) proposed to investigate wave propagation in geophysical media with an alternative seismic source: the PL source. A laser can generate a mechanical wave when hitting a target either by ablation or thermoelastic effect, whose major advantages include the non-contact and the point-like features that counterbalances the weakness of the PZT sources.

Source	Number of sources	Number of receivers
PZT	6 (divided to 7)	73 @ 2.5°
PL	8×9	109 @ 3°

Table 1: Number of sources and receivers by source type: two configurations are explored with respectively the PZT and the PL sources.

The deployment of sources and receivers using Laser Doppler Velocimetry or LDV (Shen, 2020) around the core is one of the key elements of the core-scale tomography. The configuration will have a strong impact on the uniformity and the rate of illumination inside the core by seismic probes. Experimentally, it is rather difficult to be extremely precise on the location and the effective energy of a PZT source in contact with the carbonate whereas it is straightforward with the PL source.

Tab. 1 summarizes the two source-receiver configurations that were used in our experiments. The same core slice is subjected to *2D scans*. The PZT and the PL sources are respectively applied on the same section. Fig. 2 pictures the two source-receiver deployments. The PZT source is used in Fig. 2 a), where each source is divided into 7 secondary sources according to the receiver spacing so that each secondary source is connected with a unique receiver. The PZT source is then modelled in the following way: the two external secondary sources (for example src11 and src17 in Fig. 2 a)) will be linked to most of the receivers which are located outside the cylindrical beam of the PZT; the other secondary sources (for example src12 to src16 in Fig. 2 a), only the sources with odd indices are displayed for readability) will be connected to the receiver right on the opposite side of each source. Regarding the PL sources in Fig.2, 8 aluminum flakes are stuck onto the carbonate core and each flake receives 9 distinct pulsed-laser sources. Since the laser source is punctual when well focused, it is much more convenient to model it in space as shown in Fig. 2 b), where each single source will be simply linked to all the receivers concerned. Meanwhile, Fig. 2 outlines the illumination rate inside the core by the source-receiver arrangements: they correspond actually to the rays in a homogeneous

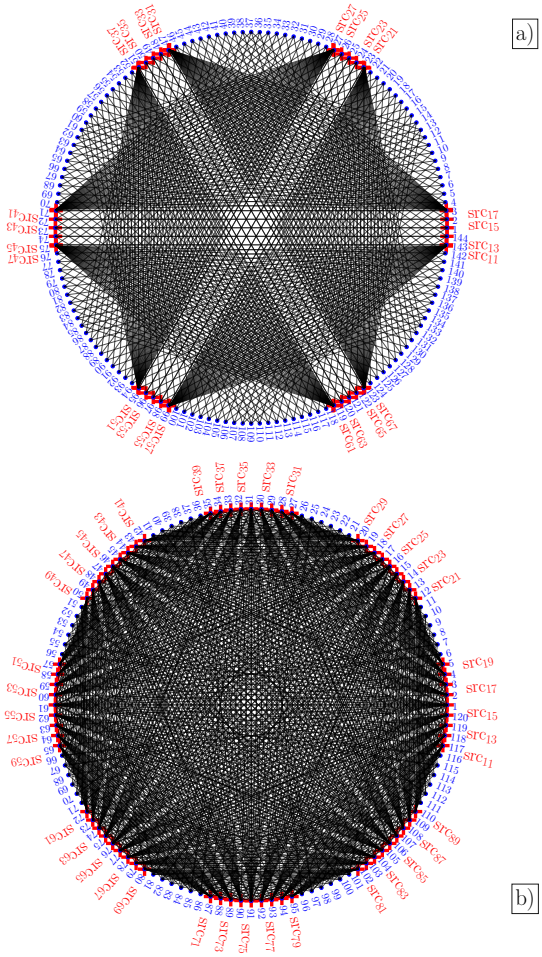

Figure 2: The two experimental configurations: a) employs the PZT source while b) features the PL source. Receivers are Laser Doppler Vibrometer laser beams for both. Obviously, a) shows lower ray densities than b). In terms of ray distribution, the PZT source seems to deteriorate the homogeneity of ray distribution along the source beam as shown in a); configuration b) featuring the pulsed-laser source shows a more homogeneous ray distribution.

medium (straight path, constant velocity).

In the case of PZT sources, the central area of the core is always poorly illuminated by ray intersection points with respect to most of the other areas in the same core since Fig. 2 a) shows that the corridors formed by the PZT beam are significantly less illuminated than the areas outside. Fig. 2 a) highlights also six weakly-illuminated shallow zones between two PZTs neighbours due to the narrow azimuth range of receivers, namely 90° for PZT source instead of 300° for PL sources. Both Figs. 2 a) and b) present very high ray densities at the vicinity of each point source, especially in a). Rays in Fig. 2 b) are better distributed than in a) due to the sparser spacial distribution of the point sources.

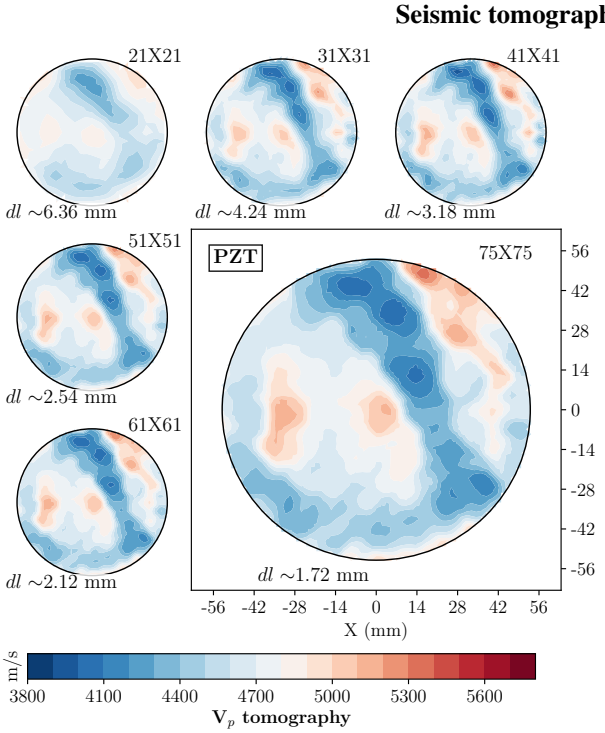

Figure 3: V_p tomography on the carbonate core slice featuring a moon-like area. The experimental configuration is depicted in Fig. 2 a), with the PZT source. The tomography grid is gradually refined to reach finally 75×75 where the grid side-length approximates 1.72 mm. A boot-like pattern is reconstructed instead. The pattern features lower V_p and is positioned differently compared to the moon-like pattern in the CT-scan.

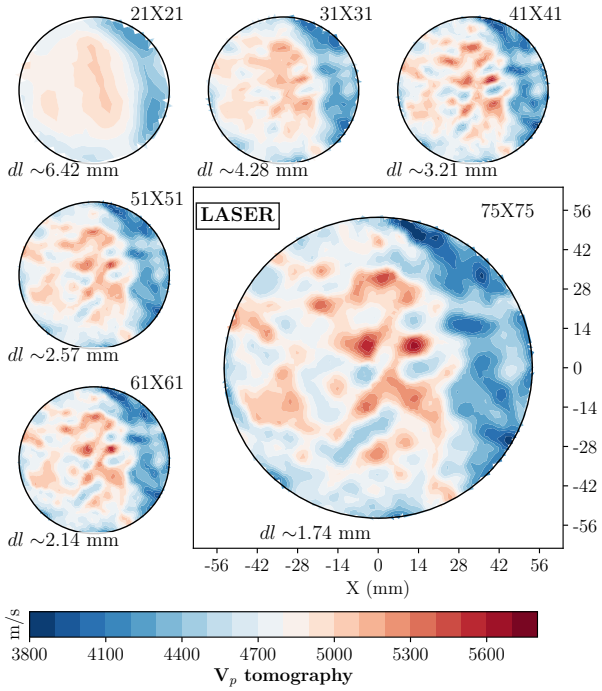

Figure 4: V_p tomography from the experimental configuration depicted in Fig. 2 b), with the PL sources. A moon-like pattern is successfully reconstructed with a relevant position.

SEISMIC TOMOGRAPHIES

A multi-level First Arrival Travel-time Tomography (FATT) tool is used to estimate the elastic V_p in the carbonate core slice. FATT is a ray-theory based (Virieux et al., 1988; Kravtsov and Orlov, 1990; Cerveny, 2005) indirect inversion method that will minimize the difference between the observed First Arrival Travel-times (FAT) and the simulated FAT. We added a multi-level feature into the tomography tool: the tomography will be performed on progressively refined multi-grids. FAT are carefully picked on the seismograms from both of the two experimental configurations and the results of multi-level FATT are shown in Fig. 3 & 4.

Fig. 3 displays six of the multi-level tomographic images from the core-probing configuration a) featuring six PZT sources and 73 receivers for each source. At first glance the images of each grid appear to have similar patterns, with a boot-like lower velocity pattern in the upper right part of the core domain. Another lower velocity area is visible in the lower part, which is connected with the boot-like pattern. Two main higher velocity areas can be distinguished: the first one neighboring the boot-like pattern on the upper right corner, the second one surrounded by the lower velocity patterns. Despite the overall similarity among the six images, local differences can be seen if we look into the details of each pattern. The outline profile of the slice is efficiently achieved after the very first multi-level iterations. The further refinement of the grid will mainly contribute to local improvement, namely the resolution on smaller objects. The whole velocity model shares some common points with the CT-scan image in Fig. 1. However, the position of the boot-like lower velocity pattern is too close to the core center compared to the moon-like pattern on the edge of the CT-scan image.

Similarly, Fig. 4 illustrates six multi-level tomographic images from the core-probing configuration b) featuring 8×9 laser pulsed sources and 12∼13 receivers for each source. Similar to Fig. 3, the images in Fig. 4 show the same outline profile, with a moon-like lower velocity pattern in the upper right part of the core domain and some patches featuring higher velocities in the center and on the left. As the grid refines, the tomography change in details, focusing on smaller and smaller objects. We can see contrast enhancement of V_p model as the grid goes finer. The whole velocity model shares good resemblance with the CT-scan image in Fig. 1. Not only the lower velocity pattern is moon-like as in Fig. 1, but also the position of this pattern is well constrained. If we look into the details of smaller patterns in Fig. 4, we see that their contours get better and better determined with the grid refinement. These detailed patterns do not always match with the patterns that can be seen in Fig. 1 b), even if some similarities express vaguely. Nevertheless, one should keep in mind that the physical quantity expressed by Fig. 1 is the attenuation coefficient to X-ray of the material, which can hold a nonlinear relation with the elastic wave velocity; the FATT reconstructed a fairly precised

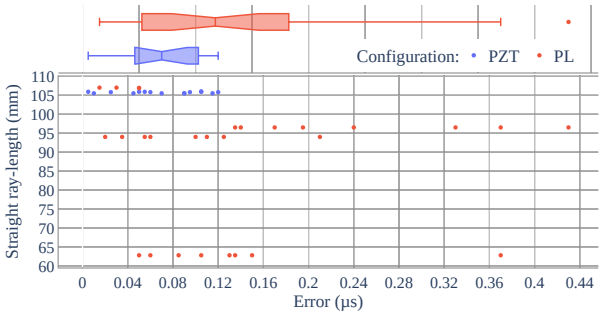

Figure 5: FAT picking error assessments by reciprocal source-receiver couples. The errors are half the absolute differences between the reciprocal travel-times. Blue scatter points and box plot correspond to the PZT source; red ones show thus the results from the PL source. The straight ray-lengths are added as an extra dimension to better distinguish the scatter points.

V_p model under the core-probing configuration b) with respect to Fig. 3 from configuration a). The resolution is considerably improved by this core-probing configuration, making the whole tomographic velocity values more reliable.

ERROR ANALYSIS

The ending of the multi-level FATT depends actually on the errors in FAT data. Here we will address exclusively the uncertainty in FAT pickings. Hermans et al. (2012); Nguyen et al. (2009) proposed and used a "reciprocal error" estimation in electric resistivity measurements, which can also be applied to estimate errors efficiently on our FAT pickings for both the two configurations of Fig. 2: among the valid source-receiver groups, there are 15 reciprocal couples in the configuration a) while 28 in the configuration b).

Fig. 5 shows that the FAT picking error medians are respectively 0.07 μs and 0.12 μs for the two configurations. These error estimations have been taken into consideration during the multi-scale FATT to avoid largely over-estimated tomography: the RMS errors yielded by the final FATT are smaller than the FAT picking error medians.

On the other hand, we can compare directly the FAT of the two configurations illustrated in Fig. 2. Even though all the rays are not comparable due to the difference of the source-receiver arrangements, nearly 90 couples of comparable rays are found, which is enough for a quantitative comparison of the FAT from the two sources. Fig. 6 displays the FAT for each comparable ray couples as well as their differences: the pulsed-laser source and the PZT source yield similar FAT curves following the comparable rays; the majority of the absolute half differences between the two are beneath 0.5 μs. This indicates that the two datasets, one from the PZT source and the other from the PL source, are consistent with each other.

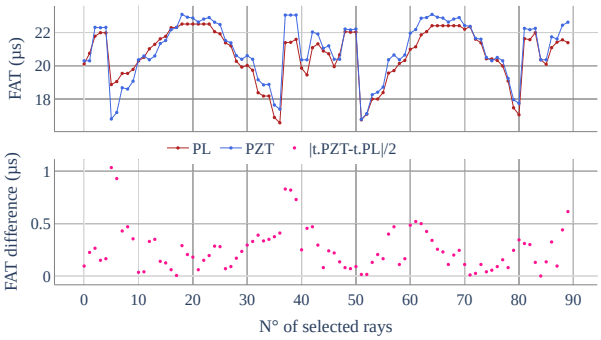

Figure 6: Differences between the FAT of comparable ray couples from the two configurations featuring respectively the PZT and the PL sources: the FAT curves follow a similar trend and the FAT differences are small (median≈0.16 μs)

CONCLUSIONS

The tomography results and error analysis show that the PL source is successfully applied onto a laboratory-scale geophysical experiment aiming at elastic V_p assessment of a heterogeneous carbonate core. The tomography result from the PL source is consistent with the X-ray CT-scan images. In parallel, a PZT source is also used in the same experimental context. The First Arrival Travel-times from the two ultrasonic sources follow a similar trend, which indicates that both of them allowed to measure correctly the arrival time of direct P-waves to a certain extent. Despite the similarity of FAT from the two datasets, the tomography result from the PZT source is different from both the one from the PL source and the CT-scan image. The lack of illumination in the PZT-beam corridors and the near-surface areas between neighbor PZT sources has certainly contributed to this difference. The flexibility of the point-like pulsed-laser source makes it more convenient to achieve a better illumination inside the medium. In addition, the modelling in space of a pulsed-laser source is straightforward, which can reduce considerably the uncertainties of source locations compared with the PZT source.

In terms of short-term perspectives, first, other seismic attributes, such as the amplitude and frequency, may be explored to estimate other geophysical properties including Quality Factor and porosity; second, more advanced inversion methods such as the Full Waveform Inversion could also be applied to laboratory-scale datasets.

ACKNOWLEDGMENTS

C. Shen wants to thank IPRA (Institut Pluridisciplinaire de Recherche Appliquée) and ED SEA (École Doctorale des Sciences Exactes et leurs Applications) of UPPA for financial support of his PhD. We would like to thank particularly TOTAL and the project ALBION for supporting this project.

REFERENCES

Backus, G. E., 1962, Long-wave elastic anisotropy produced by horizontal layering: Journal of Geophysical Research, **67**, 4427–4440.

Bailly, C., J. Fortin, M. Adelinet, and Y. Hamon, 2019, Upscaling of elastic properties in carbonates: A modeling approach based on a multiscale geophysical data set: Journal of Geophysical Research: Solid Earth.

Bretaudeau, F., D. Leparoux, O. Durand, and O. Abraham, 2011, Small-scale modeling of onshore seismic experiment: A tool to validate numerical modeling and seismic imaging methods: Geophysics, **76**, T101–T112.

Capdeville, Y., L. Guillot, and J.-J. Marigo, 2010, 2-D non-periodic homogenization to upscale elastic media for P–SV waves: Geophysical Journal International, **182**, 903–922.

Cerveny, V., 2005, Seismic ray theory: Cambridge university press.

De Cacqueray, B., P. Roux, M. Campillo, S. Catheline, and P. Boue, 2011, Elastic-wave identification and extraction through array processing: An experimental investigation at the laboratory scale: Journal of Applied Geophysics, **74**, 81–88.

Dellinger, J., and L. Vernik, 1994, Do traveltimes in pulse-transmission experiments yield anisotropic group or phase velocities?: Geophysics, **59**, 1774–1779.

Dupuy, B., S. Garambois, A. Asnaashari, H. M. Balhareth, M. Landrø, A. Stovas, and J. Virieux, 2016a, Estimation of rock physics properties from seismic attributes—Part 2: Applications: Geophysics, **81**, M55–M69.

Dupuy, B., S. Garambois, and J. Virieux, 2016b, Estimation of rock physics properties from seismic attributes—Part 1: Strategy and sensitivity analysis: Geophysics, **81**, M35–M53.

Dvorkin, J., and U. Wollner, 2017, Rock-physics transforms and scale of investigation: Geophysics, **82**, MR75–MR88.

Hermans, T., A. Vandenbohede, L. Lebbe, and F. Nguyen, 2012, A shallow geothermal experiment in a sandy aquifer monitored using electric resistivity tomography: Geophysics, **77**, B11–B21.

Holzhauer, J., D. Brito, C. Bordes, Y. Brun, and B. Guatarbes, 2017, Experimental quantification of the seismoelectric transfer function and its dependence on conductivity and saturation in loose sand: Geophysical Prospecting, **65**, 1097–1120.

Ketcham, R. A., and W. D. Carlson, 2001, Acquisition, optimization and interpretation of X-ray computed tomographic imagery: applications to the geosciences: Computers & Geosciences, **27**, 381–400.

Kravtsov, Y. A., and Y. I. Orlov, 1990, Geometrical Optics of Inhomogeneous Media: Springer-Verlag Berlin Heidelberg.

Nguyen, F., A. Kemna, A. Antonsson, P. Engesgaard, O. Kuras, R. Ogilvy, J. Gisbert, S. Jorreto, and A. Pulido-Bosch, 2009, Characterization of seawater intrusion using 2d electrical imaging: Near Surface Geophysics, **7**, 377–390.

Scales, J. A., and A. E. Malcolm, 2003, Laser characterization of ultrasonic wave propagation in random media: Physical Review E, **67**, 046618.

Shen, C., 2020, Études expérimentales et numériques de la propagation d'ondes sismiques dans les roches carbonatées en laboratoire: PhD thesis, Université de Pau et des Pays de l'Adour.

Tiwary, D. K., I. O. Bayuk, A. A. Vikhorev, and E. M. Chesnokov, 2009, Comparison of seismic upscaling methods: From sonic to seismic: Geophysics, **74**, WA3–WA14.

Virieux, J., V. Farra, and R. Madariaga, 1988, Ray tracing for earthquake location in laterally heterogeneous media: Journal of Geophysical Research: Solid Earth, **93**, 6585–6599.